



Efficient label-free CTC enrichment using novel elevated height chip chamber by vortex technology

A. Amini¹ · H. Hajghassem² · A. Nikfarjam² · N. Yarahmadi² · A. Mohamadsharif² · F. HajiMohammadHoseyni² · N. Moradi²

Received: 13 November 2021 / Accepted: 10 May 2022 / Published online: 30 May 2022
© The Author(s), under exclusive licence to Springer-Verlag GmbH Germany, part of Springer Nature 2022

Abstract

Circulating tumor cells (CTCs) are essential evidence for monitoring tumor dynamics and efficient cancer therapy. Besides its clinical importance, it is a feasible method for liquid biopsy in oncological studies. Vortex is a label-free technique using inertial microfluidic technology to separate CTCs from blood with high throughput. A possible moderate separation efficiency arises due to the loss of particles from the vortex reservoir during particle-to-particle interactions. This study develops a novel three-dimensional reservoir geometry of the vortex with more efficient CTCs separation. In the proposed geometry, the height of the main channel is the same as the vortex chips and sets to 70 μm ; however, the reservoir height increased to 100 μm . This design is called elevated height chip (EHC). The finite element simulation method is employed for optimizing reservoir height and working Reynolds number (Re). To verify the functionality of the EHC, the constant height chip design was also fabricated and showed a good correlation with the previously reported result. Both chips are tested with polystyrene beads (20, 15, and 8 μm) and MCF-7 cells. The results show 40% and 20% increase in efficiency for polystyrene beads and MCF-7 cells, respectively. Finally, it is demonstrated that 45% efficiency and 80% purity per cycle are achieved using the new proposed structure, and it is increased to 80% efficiency and 80% purity for over three cycles repetition.

Keywords 3D vortex · Circulating tumor cells · CTC separation · Inertial focusing

1 Introduction

CTCs are cancerous cells that travel in the blood. They are disseminated from tumor tissue and can seed new tumors in the other tissues, called the metastases stage of cancer (Bankó et al. 2019). More than 90% of deaths from cancer are caused by metastases (Racila et al. 1998). Thomas Ashworth, an Australian pathologist, first suggested a theory that CTCs are a fundamental prerequisite for metastasis in the mid-nineteenth century (Rostami et al. 2019). Moreover, scientists could also obtain the whole genome of a CTC with advances in next-generation sequencing (NGS) and single-cell sequencing (SCS) technologies and relate it to primary and metastatic tumors. CTC accumulation in the

blood shows the aggressiveness and may provide insight into the patient's ongoing treatment response (Riethdorf et al. 2007). CTCs enumerating serves as liquid biopsy that could be an alternative to the cancer screening method, replacing more invasive and time-consuming techniques such as tumor biopsy (Bankó et al. 2019). So, isolation and analysis of CTCs can provide a complete description of the metastatic progression to better indicate the effectiveness of targeted therapy and discover CTC properties (Shen et al. 2017; Cho et al. 2018). However, a few challenges include the purification of CTCs from other blood cells and isolating and extracting cells without destroying or losing DNA and RNA (Cheng et al. 2019).

Many existing technologies employ affinity-based capturing methods, using antibodies or aptamers binding to surface markers of cells (Karabacak et al. 2014). CellSearch (Menarini Silicon Biosystems), the first and the unique FDA-approved CTC detection system, exploits epithelial molecular adhesion molecule (EpCAM) antibody in the enrichment step (Andreopoulou et al. 2012). Monitoring the prognosis of tumor recurrence or metastasis in patients with

✉ H. Hajghassem
Hajghassem@ut.ac.ir

¹ Department of Engineering, Faculty of Chemical Engineering, Vrije Universiteit Brussel, Brussels, Belgium

² Department of MEMS and NEMS, Faculty of New Sciences and Technologies, University of Tehran, Tehran, Iran

metastatic breast, prostate, or colorectal cancer is possible by this method (Castro-Giner and Aceto 2020). Although it is an effective clinical application device, it has a comparatively low detection sensitivity. It cannot differentiate between heterogeneous tumor cells, which may involve the downregulation of target epithelial cell surface markers (Sollier et al. 2014; Che et al. 2016). This method requires cell fixation, preventing further analysis requiring viable cells for the isolated sample. CTCs are scarce cells that are less than 100 per mL of blood (Cheng et al. 2019). So, separation methods with low efficiency may cause faulty results in clinical data.

As an alternative to biophysical markers, physical properties such as size, density, deformability, optical and dielectric properties have been used (Cho et al. 2018; Cheng et al. 2019). For example, ISET (Vona et al. 2000) and ScreenCell (Desitter et al. 2011) have used porous mechanical filters to separate CTCs. On the other hand, other isolation methods have been proposed, including hydrodynamic focusing with active separation chambers and positive or negative magnetic depletion (Cheng et al. 2019). These methods usually have drawbacks such as time-consuming preparation, clogging the filter pores, and low efficiency.

CTCs are generally larger than normal blood cells. Red Blood Cells (RBC) are the most numerous cells, about a few billion cells per mL with diameters between 6 and 8 μm (Liu et al. 2019). White Blood Cells (WBC) are larger than RBCs, with an average diameter of 10–15 μm , and there are few millions WBCs per 1 mL of blood (Liu et al. 2019). However, CTCs have an average diameter of about 15–20 μm (Liu et al. 2019). The difference between cell diameters is essential for separating with inertial methods such as serpentine, spiral microchannel, vortex technology, etc. Despite the spiral channel's high efficiency for separation higher than 85% (Warkiani et al. 2014), the vortex separates the CTCs with high purity and high throughput in a low volume solution (Sollier et al. 2014).

Vortex chip includes straight pre-focusing microchannels and comes with expanded regions called reservoirs. Vortex chip traps CTCs inside reservoirs with the rotating flow called micro-vortices, induced by inertial forces at high Reynolds number (i.e., 150–250) followed by sudden downstream expansion region. Inertial forces push cells toward vortex flow in the expansion region, where particles larger than the specified threshold gain enough displacement to enter rotating streams. Vortex technology, first was introduced by Di Carlo in 2010, is a robust approach that presents high purity, high throughput, label-free, viable, and high enrichment ratio separation method (i.e., 10^3 – 10^4); however, the capturing efficiency is still a challenging issue (Hur et al. 2011). Despite the limited capture efficiency, clinical validations on 12 patients showed that vortex successfully isolated ≥ 5 CTCs/mL from 75% of patients, while CellSearch

just detected 17% samples positive from the same population (Sollier et al. 2014). Comparison of the vortex literature works is shown in Table 1, briefly.

Mach in 2012 showed 20% capturing efficiency and 40% purity of trapping 500 MCF-7 cells/mL spiked in diluted blood using $1000 \times 300 \mu\text{m}$ reservoirs (Mach et al. 2011). Che et al. (2013) presented a high correlation between MCF-7 and 15 μm beads with almost 20% capturing efficiency and more than 80% purity using $720 \times 220 \mu\text{m}$ reservoirs. Also, they showed 47% capturing efficiency for 20 μm beads. Sollier et al. (2014), characterized vortex capturing behavior concerning flow rate. Maximum capturing efficiencies for both 19 and 15 μm beads were 60% and 22%, respectively, occurring in 6 mL/min ($\text{Re} = 210$), while for suspended MCF-7 in PBS sample was 21% in 4 mL/min ($\text{Re} = 160$) (Sollier et al. 2014). Che et al. attempted to enhance vortex capturing efficiency by optimizing the total number of serialized and parallelized reservoirs and interconnecting channel length. This design which is called Vortex HT earned 62% capture efficiency for 20 μm beads and 22% for MCF-7 10 \times diluted blood, which was increased to $\sim 36\%$ by reintroducing waste (Che et al. 2016). The high number of serialized reservoirs increases back pressure and deforms the chip causing its lifetime reduction. Also, since cells are elastic material and highly deformable, high-pressure separation has a negative effect on efficiency, so increasing efficiency for particle samples is higher than cell samples in Vortex HT. Vortex HT device reached 80% capturing efficiency after seven sample reintroducing cycles; however, due to extended run time and other practical circumstances, 45% capturing efficiency after 3 cycles were obtained as practical sample cycle in Vortex BioScience System. Paiè et al. (2017) introduced an engineered reservoir with two parallel rotation orbits inside the cavity by inserting a separation wall along the particles' pathway to decrease particle–particle interaction between trapped particles. The device showed 65% efficiency for 20 μm rigid polystyrene beads versus 50% for the standard vortex chip (Paiè et al. 2017). At the last commercialization step, the Vortex chip was fabricated on a different material (Lemaire et al. 2018) due to the high deformability of PDMS. The new PMMA chip could reach 80% in the separation of MCF-7 cells with triple sample reprocessing.

However, all the literature works demonstrate the 2D design of the Vortex chip, and it has not been studied how the out-of-plane forces could improve the trapping mechanism. Hence in this work, we propose a new three-dimensional cavity vertical flow device that enables unique capturing efficiency for MCF-7 cells. The proposed device has a lower number of serialized reservoirs to decrease the backpressure and deformation of the chip and with an enormous volume to increase the particle capacity of reservoirs. Also, its larger height along the expanded region causes

Table 1 Brief information about the remarkable Vortex technology publications since 2011

References	Change	Efficiency	Details
Hur et al. (2011)	First design 5 reservoirs in a row 8 parallel channels	23% (MCF-7 cells)	Asymmetric reservoir design
Che et al. (2013)	Symmetric reservoir Total reservoir dimension to 720×480 μm reservoirs	20% Capturing Efficiency 80% Purity	4 reservoirs in a row 16 parallel channels
Sollier et al. (2014)	8 parallel channels 8 Reservoirs in a row	Up to 60% (19 μm microparticles) 21% (MCF-7 cells)	4 mm pre-focusing channel Different channel cross-sections dimensions
Che et al. (2016)	12 reservoir in a row 16 parallel channels	45% separation in triple processing 80% efficiency in 7-time reprocessing	Optimizing the reservoir number and pattern for the maximum efficiency
Paiè et al. (2017)	12 Reservoirs in a row 10 parallel channels Columned Reservoirs with a 720*1350 μm	65% efficiency in one step processing	Optimizing the dimension of the column
Lemaire et al. (2018)	8 reservoirs in a row 16 parallel channels	60% processing in a single-step process Up to 80% in a 3-step processing	Study on-chip material rigidity Introducing a new platform, VTX-1, for automated sample processing
Haddadi et al. (2018)	Simulation and experiment on reservoirs with different aspect ratios	–	Study on the flow specification in simulation and experiment in a confined reservoir, defining the cavity capacity and study on separatrix breakdown
Rastogi et al. (2021)	Orthogonal outlet 720*480 μm reservoir 3 parallel channels 3 reservoirs in a row	Not mentioned clearly	–

multi-stable orbits with reduced particle–particle interaction. In addition, to choose optimized design parameters, a semi-theoretical method combined with previously reported experimental phenomena was adopted. Separatrix boundary location, vortex shape within the cavity, the magnitude of shear rate, and trapping time were enlisted as optimization parameters. Moreover, cavity capacitance, capturing efficiency, and purity of the new design were measured for both polystyrene beads and MCF-7 cells, and the results were compared to the CHC vortex chip. The newly developed device shows good consistency for MCF-7 and polystyrene bead trapping behavior over a higher Reynolds number range, while the standard control vortex chip shows low capturing for MCF-7 cells.

2 Vortex technology and device design

Vortex technology was developed as a microfluidic platform to quickly isolate intact CTCs from whole blood using inertial microfluidics and microscale vortices. Micro-vortices form as soon as a high inertia fluid inside a narrow microchannel suddenly jets into an expanded reservoir connected to another narrow microchannel (Fig. 1a). In the case of high fluid inertia, the relative low-pressure region forms nearby the cavity entrance while the high-pressure region

forms near the cavity outlet. This pressure gradient detaches the streamlines near the outlet (trailing wall) and forms isolated circulating streams inside the cavity. Channel Reynolds number (Re_c) is a dimensionless parameter defined as a ratio of inertial to viscous forces.

$$Re_c = \rho U_m D_h / \mu. \quad (1)$$

Moreover, the Particle Reynolds number is defined as the following relation.

$$Re_p = Re_c \left(\frac{a_p}{D_h} \right), \quad (2)$$

where D_h is the characteristic channel diameter, ρ is the fluid density, U_m is the maximum velocity, μ is the dynamic viscosity, and a_p is particle diameter. At particle Reynolds number (Re_p) > 1 and $a_p/D_h > 0.07$ (i.e., when the particle diameter is noticeable compared to the channel diameter), inertial focusing takes place, and particles focus at the center of the broader face of a rectangular cross-section (For instance, a 10 μm particle in a 40*70 μm channel). The entering narrow microchannel focuses the particles in two stable equilibrium positions and prepares the particle to take the maximum possible effect from the unexpected geometry changes (Fig. 1a). The shear gradient lift force directs particles toward the

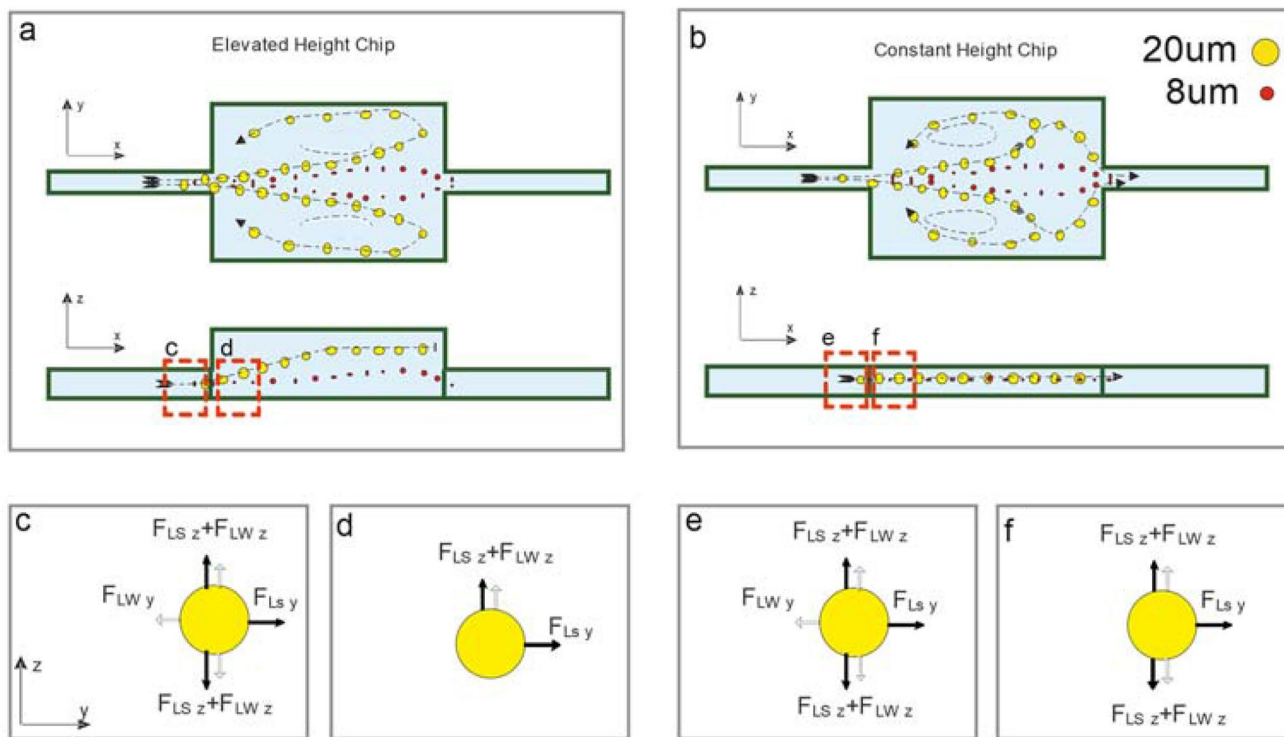


Fig. 1 Chip design inspired from Vortex HT reservoirs; **a** trajectory of 8, 20 μm microparticles in the EHC design. The reservoir height is 110 μm, and the channel height is about 70 μm. **b** Vortex HT reservoir (CHC) in the same flow rate with a constant height of about 70 μm. Shear and wall-induced forces on the particles in **c–f** areas in red boxes are shown in **c–f**, respectively, to compare forces in the Y and Z directions. Shear-induced lift forces and wall-induced lift forces are shown with black and white arrows, respectively, in **c–f**

schematics. Microparticles have a vertical displacement in the proposal design. When they enter the upper part of the reservoir, their speed will be reduced soon, and the up straight path is close to continuing. Thus, they are forced to orbit in the vortex and cannot return to the main flow stream because of the high difference in flow speed between the two parts of the reservoir. Also, in the EHC design, the space for the particles is wider to orbit on the z-axis. Hence, there could be non-planar orbits that could carry the particles

channel wall while it repels by counteracting wall-induced lift force. The overall forces form an ordered train of particles at approximately 0.4 channel diameter away from the wall. Moreover, the wall force is abruptly eliminated when a particle enters the cavity (Fig. 1a). Therefore, the shear gradient lift force (F_s) accelerates the particles toward the vortex region with no resistant force except stokes drag. F_s can be defined as:

$$F_s = f_L \rho U_m^2 a^4 / H^2, \tag{3}$$

where f_L is defined as a non-dimensional lift coefficient that is a function of the Reynolds number and the normalized cross-sectional position. Since F_s scales with a^4 (Di Carlo 2009). Therefore, only larger than the threshold size particles may have enough lateral displacement to cross the separatrix boundary and enter the vortex region (Liu et al. 2016). When a particle enters the vortex region, it experiences inertial and momentum forces and forms a stable limit cycle orbit.

In the CHC vortex chip, the particles entering the chamber are affected with a balanced force containing shear gradient and wall-induced lift force from sidewalls. As the particle enters the reservoir, the wall-induced force is suddenly removed, and the particle experiences a net-force perpendicular to the flow, which leads it through the chamber. Meanwhile, a new balance would be formed, and the particle orbits in the chamber at a specific height, as shown in Fig. 1b. However, in the EHC design, there are more forces in touch with the particle. The conventional forces in CHC also play the dominant role in EHC design; however, new forces would appear and alter the mechanism effectively. Wall-induced forces are present from the sidewalls and the top and bottom walls due to the considerable size of target particles.

On the other hand, shear-induced forces contain horizontal and vertical components because of the 3D surface of the velocity profile in the channel cross-section. However, in the conventional CHC, the vertical force was not employed. In

the EHC design, the vertical force component causes a vertical movement of particles in the reservoir and an asymmetric shape in orbiting path. This out-of-plane net force makes the particle move more facile and easier to get out of the mainstream and keeps it more stable in the reservoir. This vertical movement presents a new space with a higher volume and lower high-pressure region near the walls. It enables the particle to change its altitude in the reservoir continuously. Hence, there would be more space in the EHC device for the particle to orbit than CHC, which is limited to a specific orbit in the reservoir and reduces the particle–particle effect.

The separatrix region is one of the remarkable factors for evaluating each design at different flow rates. Separatrix is the largest vertical distance that a passing particle deviates from the main streamline without entering into the vortex. As shown in Fig. 3a, particles smaller than a threshold move upward in the flow, and the flow draws them into the outlet and finally exits from the reservoir. Particles that pass vertically from this zone would enter the orbit and return to the reservoir entrance. The flow rate at the most achievable efficiency is defined as critical Reynolds. After injection of all samples, a buffer solution with the same Re is injected into the channel as a substitution for sample solution to wash unmeant minor debris contamination while larger particles maintain their orbits (Khojah et al. 2017). Later, controlled releasing of trapped particles is achieved by reducing the flow rate, eliminating the vortex, and providing uniform laminar flow inside the cavity to wash out trapped cells (Fig. 1).

We used two microfluidic chips and tested for CTC separation from the buffer. The geometry of CHC originates from maintaining the layout of the Vortex chip. This design consists of 16 parallel channels (i.e., separated by a 1 mm gap) with an arrangement of six reservoirs along each channel. The reason behind using six reservoirs in each channel is the high effect of pressure resistance in the separation behavior of each reservoir. Sollier's results (Sollier et al. 2014; Lemaire et al. 2018) show that the flexible PDMS chip has lower capturing efficiency than rigid PMMA chips. Furthermore, it shows that the last four reservoirs of PDMS chips (since they experience low pressure) have around 70–80% capturing capacity. So, we chose six reservoirs to optimize the design. The dimension of each reservoir is $900 \times 300 \mu\text{m}$, and the main channel has $70 \mu\text{m}$ height (h) and $40 \mu\text{m}$ width (w). In EHC, the height of the reservoir is increased to $110 \mu\text{m}$, while other parameters were considered the same as the CHC design (Fig. 1).

3 Materials and methods

3.1 Chemicals

A negative photoresist, SU-8 2050 (MicroChem, MA, USA), was used to make the mold by UV lithography on a 4-in.

Si wafer. Sylgard 184 Polydimethylsiloxane (PDMS) was procured from Dow Corning (Midland, MI, USA). Glycol Methyl Ether Acetate (PGMEA) is used as SU-developer. Standard microbeads from Phosphorex (Hopkinton, MA, USA) in three different average diameters of 8, 15, and $20 \mu\text{m}$. MCF-7 cells were cultured in DMEM medium; fetal bovine serum (FBS) and penicillin–streptomycin (Invitrogen) were acquired. These chemicals were purchased from Sigma-Aldrich (Taufkirchen, Germany).

3.2 Device fabrication

Two microfluidic chips (i.e., CHC and EHC) were fabricated using SU-8 mold and PDMS for replica molding. The SU-8 master mold was made on a silicon wafer using the conventional UV lithography method. CHC device was fabricated based on the procedure mentioned in Dhar et al. (2015) by applying and spinning SU-8 photoresist on a Si wafer to obtain $70 \mu\text{m}$ resist thickness and following with pre-baking of photoresist. UV-light was then exposed to the photoresist followed by post-exposure-bake, and finally, SU-8 was developed using Propylene Glycol Methyl Ether Acetate (PGMEA) as shown in Fig. 2a step 1 to 4.

The EHC chip was fabricated using two-step lithography, as shown in Fig. 2. In the first step, a $70 \mu\text{m}$ layer of SU-8 was spin-coated on a Silicon wafer. The first design step, which contained the chip's geometry, inlet, and outlet, and 16 microchannels were fabricated on the substrate exposed to the UV light and then developed. In the second step, a $110 \mu\text{m}$ layer of SU-8 was spin-coated on the previous geometry, followed by a second mask alignment using the former geometry, then baked and exposed to UV light. After developing, the microfluidic mold was ready to use.

The PDMS chips were fabricated using replica molding. PDMS and the curing agent were mixed with a ratio of 10:1, respectively. The final mixture was applied to the master mold and degassed, then placed in the oven at $80 \text{ }^\circ\text{C}$ for 2 h to cure. The cured PDMS was peeled off from the master mold; formerly, inlet and outlet holes were punched by a 2 mm biopsy punch. After exposure to oxygen plasma for 30 s (Henniker HPT-100, NH, USA), the PDMS and a glass sheet were bound.

3.3 Sample preparation

Fluorescent polystyrene particles were utilized with mean diameters of 8, 15, and $20 \mu\text{m}$. 0.1% Tween 20 also was added to particle suspensions to prevent particle aggregation. Two experiments were designed to show the difference between the two chips with various concentrations of solutions. In the first experiment, $20 \mu\text{m}$ particles with different concentrations were injected into both chips to compare the performance. In the other experiment, solutions containing

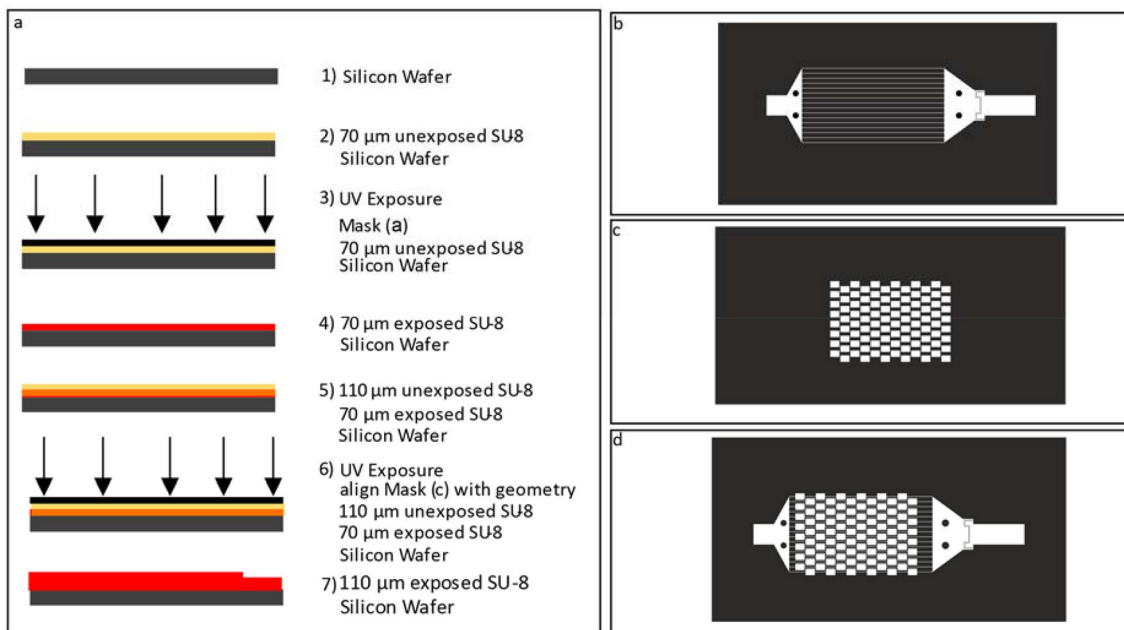


Fig. 2 Device fabrication **a** steps of SU-8 mold fabrication with multiple heights, **b** the first mask geometry for 70 μm height region, **c** the second mask geometry for exposing on 110 μm layer in the EHC vor-

tex chip and **d** exhibits the geometry of CHC (vortex HT) chip with 70 μm height

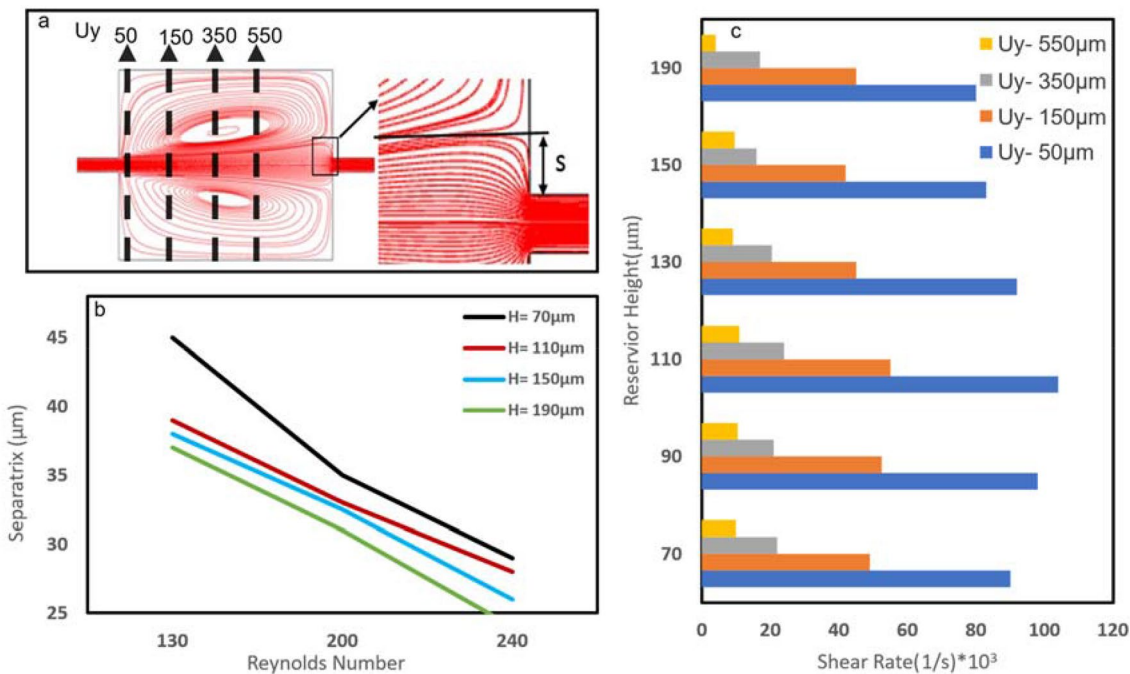


Fig. 3 Vortex morphology and separatrix boundary. **a** Streamline of fluid in reservoir area in $Re = 130$ and separatrix boundary. The separatrix width is shown by S . **b** 2D plot of Re and separatrix boundary

in different heights of the reservoir; **c** maximum of shear rate in the different heights of the reservoir with 50, 150, 350, and 550 μm distances from the leading wall

8 μm and 20 μm were injected into both chips. As mentioned before, deionized water was used for the buffer solution in all the samples.

Also, MCF-7 cells were cultured in a DMEM medium. The medium was supplemented with 10% fetal bovine serum and 1% penicillin–streptomycin incubated at 37 °C under 5% CO_2 . Cells were passaged once they reached 80% confluence, then fixed by 1% glutaraldehyde and spiked in PBS solution. A high concentration of the sample (with 2000 particles or cells) was used for saturation tests, and a low concentration (50–150 particles or cells per mL) was used for capture efficiency and purity tests.

3.4 Experimental setup and methods

An adjustable syringe pump was used to control fluid flow. In all the experiments, a digital camera with a high shutter speed (Canon D700) was mounted on the microscope (Nikon Ti-U) to analyze the trapping and releasing processes. The sample on the microscope was illuminated by a mercury arc lamp with a 10 \times and 4 \times objective lens. The minimum shutter speed of 1/4000 was used to investigate vortex formation and the particle motion in reservoirs. The fluorescence images were captured by a CCD Coolsnap HQ2 camera (Roper Scientific, Evry, France), then processed by Zen2 software.

Before injecting particle suspensions, the chip was primed with DI water with an optimized flow rate for each chip to form the vortex streamlines and eliminate microbubbles in reservoirs. Promptly, the Particle suspension was injected into the channel to separate from the entire solution. Then, DI water was pumped into the channel again for 30 s to ensure all particles had entered the device. In the last step, by decreasing the flow rate ($\text{Re} = 5$), trapped particles were released from the reservoir and collected in a 96 well-plate for final analysis. Samples were mixed by vortex shaker to avoid particles to sediment before each step to preserve a uniform distribution of particles.

For the capacity test, 6 mL solution of 2000 particles per mL of 20 μm size particles was used. On the other hand, two solutions with concentrations of 50 and 150 particles/mL of 20 μm size particles were used for efficiency analysis. Homogeneous mixtures of 8, 15, and 20 μm particles were utilized to study the purity. Also, the same procedure was used to quantify the capacity of the MCF-7 cells in the device, and 6 mL of a sample of 100 cells/mL was used to analyze trapping efficiency in both chips.

3.5 Simulation

Both designs were simulated by COMSOL Multiphysics 5.2 (COMSOL, Burlington, MA) to investigate the streamlines' stability and velocity distribution in the micro vortex flow.

Laminar flow physics was applied in a single-phase flow regime. Water was used as the carrier fluid with a density (ρ) of 1000 kg/m^3 and dynamic viscosity (μ) of 10^{-3} kg/m s . The effect of reservoir height was investigated by simulating different reservoir heights (i.e., 70, 90, 110, 130, 150, and 190 μm). The microchannels connected to the reservoir contained a 500 μm length for each inlet and outlet. The flow was introduced to the channel by applying a fully-developed flow to satisfy the practical situation. The inlet flow rate was altered from 10 to 500 $\mu\text{l/min}$ for a single channel in different steps to observe the best situation of the velocity, separatrix region, shear gradient force, and the vortex flow geometry results for the optimization. The flow Reynolds was measured by evaluating the mean channel velocity. Also, the results were validated by comparing the vortex shape in the fluorescent images of orbiting microparticles and the streamlines in the simulated reservoir at the same flow rate.

4 Results and discussion

4.1 Simulation and optimization

Vortex simulations in previous studies were performed using two different methods, including direct numerical simulation (DNS) and conventional CFD. DNS uses Lattice–Boltzmann Method (LBM) (Haddadi and Carlo 2017; Haddadi et al. 2018) and uses complex computations, but is not sufficiently consistent with the experimental results for separating CTC from blood due to the complex pathway of particles considering their interaction. Also, DNS is a time-consuming simulation process. Most importantly, particle–particle interaction is not considered in these methods (Jiang et al. 2018). So numerical solutions are not reliable to obtain precise results.

The analytical CFD method was adopted in this work, and parameters were investigated in the conventional simulation method. We studied four parameters to obtain optimum cavity geometry in two groups. The first group relates to the physical variables of the vortex, including the vortex morphology and the separatrix width. The second parameters group employed force-dependent variables, including shear gradient lift and residence time of particles. Vortex formation starts at a low Reynolds number (i.e., $\text{Re} = 30$) from the beginning of the reservoir, called the leading wall, in the form of an incomplete triangular vortex cell. Increasing flow rate increases the Reynolds number of flow, and the vortex shape progressively expands and fills the cavity (Fig. S1). A complete flow cell is formed when a vortex covers the whole length of the cavity.

The effect of cavity aspect ratio and Re on the number of entrapped particles has been investigated in previous works (Haddadi and Carlo 2017; Paiè et al. 2017; Haddadi

et al. 2018). It was shown that for each reservoir aspect ratio (defined as λ), the number of entrapped particles is maximized at a specific Re , called Re_{max} . Haddadi studied the λ effect on vortex formation and showed that the number of particles inside the cavity increases by increasing the cavity length, and Re_{max} shifts to higher values while the vortex center shifts longitudinally (Haddadi and Carlo 2017; Haddadi et al. 2018). Similarly, the entrapped particles increase by increasing the reservoir width; however, no significant change in Re_{max} (vertical shift) would be observed (Haddadi and Carlo 2017). While Re_{max} increases the flow rate, more advanced test equipment and stronger channel bonding would be needed for testing. This work shows that by increasing the height of the cavity, the chip can increase the particle trapping at a lower Reynolds number, as shown in Fig. 1. The obtained results in Sect. 4.4 show the efficiency improvement of this modified geometry. To obtain optimum reservoir height and proper Reynolds number, their effect on residence time, shear gradient lift, and separation boundary were examined.

In our simulations, the reservoir shows distinguished vortex geometry due to the reservoir height at the same flow Re . As shown in Fig. S1, the vortex cells reach the critical Reynolds depending on the chamber height. The Re_{max} for 70, 110, and 150 μm reservoirs were obtained at 200, 150, and 100 Re respectively. The results represent the vortex cell forming and progress by streamlines compared to experimental images. Simulation results were validated by the vortex shape of the fluorescent beads orbiting the chamber in experiments and the obtained streamlines. Figure 1 and Fig. S1 demonstrate some evidence of the verified geometries of simulated models. However, the CHC device could

be more explicit proof of the orbiting particles in the 2D ring and closer to the simulated model because of its in-plane orbits. On the other hand, the EHC formed 3D orbits for particles and poses a different shape than the 2D simulated streamlines and remains close to the 3D streamline in simulation. Overall, the simulation results were verified by the geometrical properties of the vortex comparing to the experiments results.

The separatrix width is the minimum lateral displacement of particles needed to enter vortex flow and be trapped (Fig. 3a) (Haddadi et al. 2018). Increasing the reservoir height would decrease the separatrix width (Fig. 4b), and the probability of trapping particles increases. Figure S1 demonstrates vortex flow formation at different channel heights, and it shows that vortex flow forms at a lower flow rate with increasing channel height. Residence time is considered when a particle moves across the reservoir from the leading wall to the trailing wall. Having a more significant residence time (the lower particle speed) results in experiencing higher total shear gradient lift force, higher lateral motion of the particle toward the core of the vortex, and a higher probability of trapping. As a result, increasing channel height increases particle traveling time and trapping probability.

Another critical parameter is the shear gradient lift force (F_s). This force is directly related to the shear rate (i.e., Eq. (3)); the magnitude of F_s could be estimated by analyzing the shear rate. When a particle approaches the trailing wall, the shear rate induced force on the particle will reduce. Figure 3a shows four different positions of shear rate measurement, and Fig. 3c shows these measurements for different reservoir heights. Simulation results show that 110 μm height has a higher shear rate than other heights. Decreasing

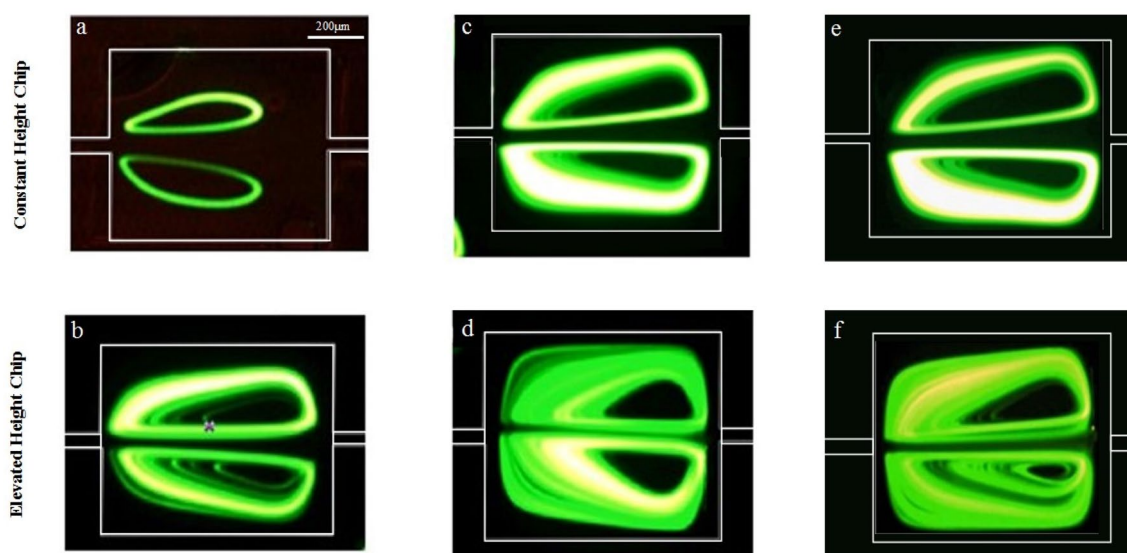


Fig. 4 Tracking pathway of 20 μm fluorescent particles in CHC and EHC (new chip); **a, b** $Re=80$, **c, d** $Re=150$, **e, f** $Re=170$

the shear rate at heights higher than 110 μm may be due to the reduction of the overpressure and the stagnation of the flow. This reduces vertical flow magnitude in the Z direction compared to the lateral flow. Conclusively, the optimized height is chosen as $H_c = 110 \mu\text{m}$ because it shows higher F_s and has smaller separatrix width and higher traveling time regarding the formation of complete vortex in lower Re .

4.2 Stable orbits

Flow condition forms a limit cycle or stable orbits for specific particle size (Haddadi and Carlo 2017; Shen et al. 2018a, b). Simulation of particle trajectories shows that particles spiral towards a unique limit cycle orbit (Shen et al. 2018a, b). The motion of an isolated particle on the limit cycle trajectory continues without deviation unless hydrodynamic interaction with other particles perturbs it. An equal amount of centrifuge and shear-induced lift force make the stable particle orbit. Collisions between multiple entrapped particles generate deviation from stable limit cycle orbit, and due to random mass exchange, particles may exit the cavity. This depletion depends on the number of particles inside the cavities. Particles may leave the limit cycle by collision with one another or because of lift force at inertial flow, which generates a lateral migration towards the recirculating flow. As the reservoir volume increases by increasing the height, more stable cycles appear and entrap more particles in different levels of Z-direction, which we call 3D vortex orbits.

The experiment results are in agreement with our simulations and indicate that elevating reservoirs height increases the reservoir capacity for particle trapping until an optimum height. The designed EHC and the CHC chips were tested for Re of 80 (Fig. 4a, b), 150 (Fig. 4c, d), and 170 (Fig. 4e, f). The vortex flow formation is a validated simulation result of

Fig. S.1. EHC streamlines in $Re = 170$ seem denser, and particles experience smaller radius trajectories than $Re = 150$; the balanced forces in the vortex containing centrifugal and the shear gradient force might be unbalanced. Hence, the particle could exit the vortex trajectory, and the efficiency decrease (Jiang et al. 2018). The following section's result shows EHC chip has a higher trapping efficiency in $Re = 15$. A comparison of CHC and EHC florescent imaging shows the number of stable rotation circuits has increased and are more efficient in EHC design. Furthermore, separatrix width is reduced, which is consistent with simulation results.

4.3 Saturation reservoir capacity

Although particle entrapment inside cavities can be controlled by the flow rate (Re), it also depends on the size of particles and saturation reservoir capacity. Expanding the volume of the reservoirs is a way to increase the number of trapped particles. We injected 20 mL of 20 μm beads and MCF-7 cells containing 2000 cells or particles at various flow rates (Re) to investigate the particle entrapment process. Lemaire showed that the reservoir capacity changes gradually in a single channel longitudinally because of PDMS deformation, and so the last reservoir has the most probability to trap the cells (Lemaire et al. 2018). We analyzed reservoir capacity by taking images from three different regions beginning, middle, and the end of the channel by A, B, and C, as shown in Fig. S.2, respectively. For instance, Fig. 5a and b show trapped beads in the first and middle reservoirs.

Figure 5c shows the number of particles trapped, and as we can see, the reservoir capacity in our proposed chip (i.e., EHC chip) is higher than the CHC. It is noteworthy that the CHC design reaches the critical Re in higher flow rates because of its reservoir geometry than the EHC design. The

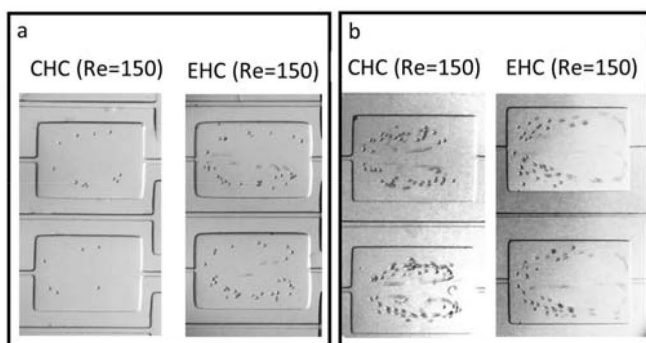
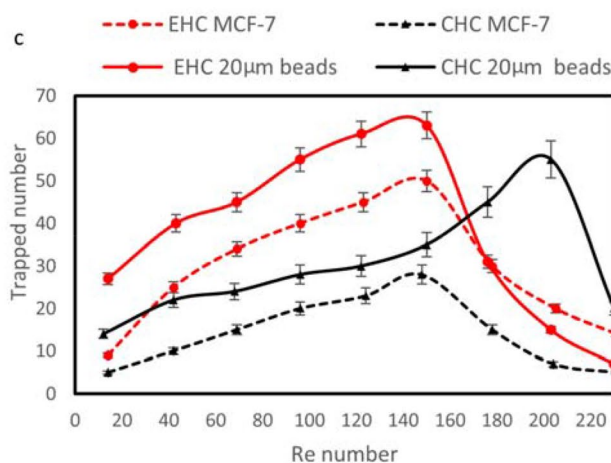


Fig. 5 Saturation reservoir capacity. **a** 20 μm polystyrene microparticles in $Re = 150$ at the region A and **b** for the region B for both chips (control chip (CHC) and new chip (EHC)) with 2000/mL particles.



c Number of entrapped 20 μm and MCF-7 cells in each reservoir for EHC and CHC at the middle section in different Re

comparison between the two approaches in our tests clears that the reservoir's 3D geometry has a remarkable effect on the trapping mechanism. So, altering the geometry tends the reservoir to separate more particles/cells at lower Re . The EHC design represents the peak performance at about $Re = 150$ compared to the CHC device at $Re = 200$ for $20\ \mu\text{m}$ microspheres.

Maximum reservoir capacity takes place at ($Re_{\text{max}} = 150$) for the proposed chip (EHC) and at ($Re_{\text{max}} = 200$) for the CHC, which is consistent with simulation results. The new chip traps more particles at section C than the CHC and has a larger quantity for particle saturation. Sollier showed that the trapping efficiency for particles with different sizes is different at various Re (Sollier et al. 2014). So, both chips were tested with $15\ \mu\text{m}$ and $20\ \mu\text{m}$ particles and MCF-7 cell line, and the result is shown in Fig. 5c, and Fig. S.3, which is in agreement with the results reported by Sollier. The maximum number of $20\ \mu\text{m}$ and $15\ \mu\text{m}$ trapped beads for the CHC are 55 and 32, respectively, at $Re = 200$, while the maximum number of MCF-7 trapped cells is 20 at $Re = 150$, and it happens because of the deformation of cell and its effect on particle–particle collision (Haddadi et al. 2018).

However, trapped beads and cell samples show the same behavior in the proposed chip (EHC, Fig. 5c). The maximum number of trapped $20\ \mu\text{m}$ and $15\ \mu\text{m}$ particles and MCF-7 cells at $Re = 150$ are 60, 23, and 50, respectively (Fig. S4). So, the trapping peak of cells and microparticles are achieved at the same Re number in this work, which is crucial for cell separation from the blood. More stable orbits and lower particle–particle collision could be the reason for this improvement.

4.4 Capture efficiency and purity

Purity and enrichment ratio are the main advantages of the vortical flow separation (Sollier et al. 2014; Che et al. 2016). The separation mechanism is extremely size-dependent (Wang et al. 2016). The induced lift force is theoretically unable to entrap the smaller particles from the main flow. In the previous papers (Mach et al. 2011; Sollier et al. 2014; Che et al. 2016), many smaller particles were observed orbiting in the reservoirs because of the high concentration of particles/cells in the flow. Meanwhile, the washing step would exit them from the reservoirs. They orbit in the vortex region unstably, and afterward, most of them are thrown out of the vortex (Che et al. 2016, Haddadi and Carlo 2017, Haddadi et al. 2018; Shen et al. 2018a, b). Haddadi showed that the removal effect for smaller particles might be the effect of particle–particle interaction (Haddadi and Carlo 2017). Altogether, the presence of smaller particles is low in this method.

Capture efficiency is the most critical factor for CTC separation. From the beginning of vortex technology, most of

the studies were aimed to improve capture efficiency. These studies contained altering channel width (Mach et al. 2011; Sollier et al. 2014; Dhar et al. 2015; Haddadi and Carlo 2017), channel height (Zhou et al. 2013; Sollier et al. 2014), channel serialization (Hur et al. 2011; Che et al. 2016), changing the reservoir aspect ratio (Haddadi and Carlo 2017; Shen et al. 2018a, b), changing the outlet direction (Wang et al. 2013; Rastogi et al. 2021), and changing the chip material (Lemaire et al. 2018; Volpe et al. 2019). The Vortex HT obtained the best clinical result, lower than 60%, after twice recycling the outlet (Che et al. 2016). On the other hand, the last and the best vortex cell separation device, VTX-1, was proposed using a rigid plastic chip and achieved 80% capture efficiency (Lemaire et al. 2018).

We believe that in previous works there was not enough attention paid to the reservoirs' third axis expansion. As described in Sect. 2, the effect of the vertical net force is remarkable due to the result of our simulations and experiments. The particle passes through the reservoir with a velocity approximately equal to the flow (about 4.5 m/s). Therefore, the particles have just few millisecond time to cross the mainstream borders and enter the orbiting streamlines. Affecting the vertical force in the EHC chamber could move the particle more effectively than the 2D mechanism. That is due to lower velocity of flow in the expanded height of the chamber compared to the channel. Nevertheless, in the CHC design, the Re number of the flow is higher, and the passing time is less than the proposed design. Moreover, the orbiting particles in the chambers are not just in a 2D plane and have more space to orbit without much interaction with others, as shown in Fig. 4. In the CHC design the particles are focused around a ring at a middle height of the reservoir and it saturates fast (Hur et al. 2011).

To measure capturing efficiency, three different concentrations of $20\ \mu\text{m}$ particle were prepared. 300, 600, and 900 particles were diluted in 6 mL of water. Figure 6a, b show the last reservoirs of both chips with their trapped particles for different samples (Lemaire et al. 2018), and it shows that the new EHC traps more beads than CHC. A similar test by MCF-7 samples (600 cells/mL) was run. In Fig. 6c, the yield capacity of both chips is shown for different concentrations of beads and one concentration of MCF-7 cells. The new EHC and CHC efficiency for MCF-7 cells is measured at 45% and 19%, respectively. Also, for $20\ \mu\text{m}$ beads, we obtained the separation efficiency of 75% and 55% for the EHC and the CHC, respectively. We believe that this considerable increase in efficiency is due to the larger orbiting space, lower possibility of collision, and better trapping elements.

For increasing the separation efficiency, recycling the chip's outlet and reintroducing it into the device is done twice (Che et al. 2016). In Fig. 6d, the cyclic behavior of EHC and CHCs is shown. CHC reaches 45% efficiency for cell samples in 3

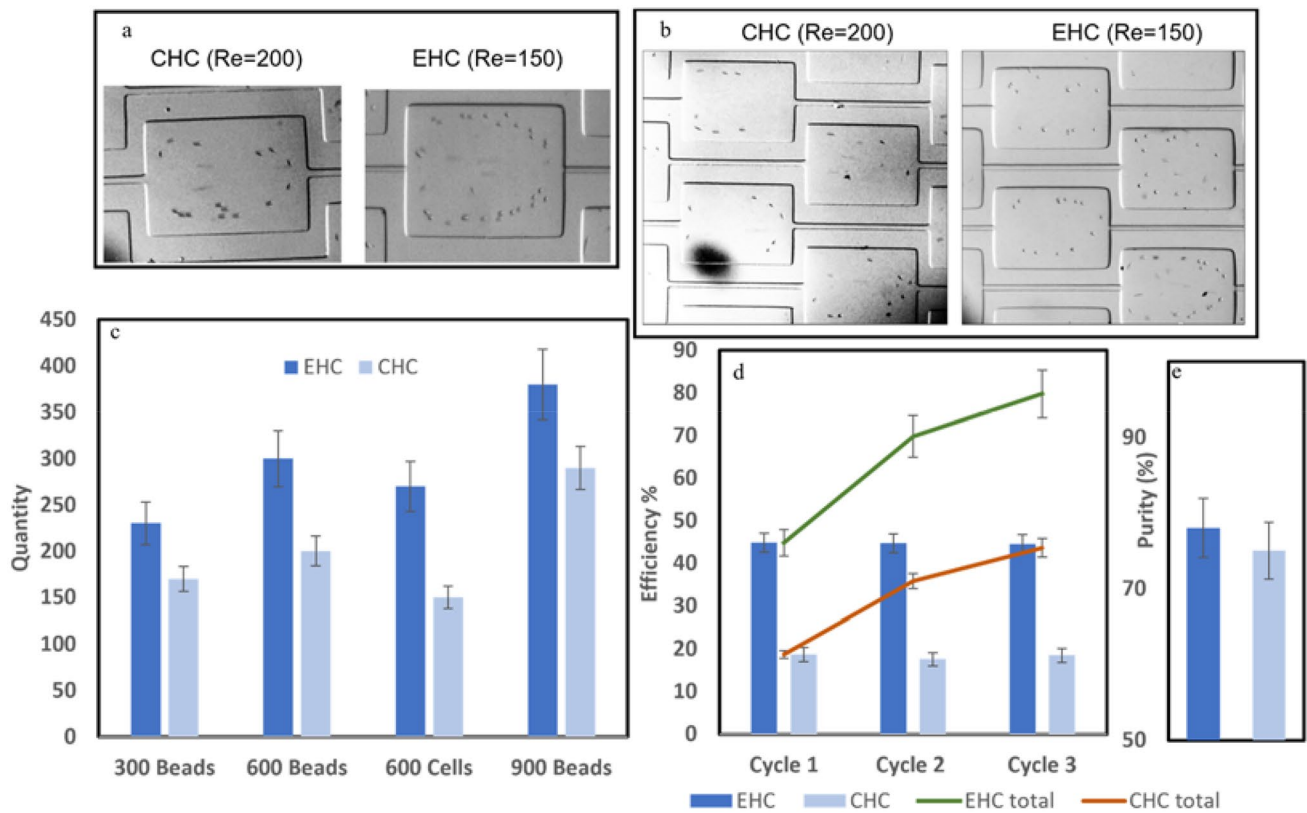


Fig. 6 Comparison of the number of particles and cells trapped in both chips. **a** Sample: 6 mL of 50 particles/mL. **b** Sample: 6 mL of 150 particles/mL. **c** Shows the number of captured beads, with the two devices varying the number of processed beads. Note that the new device always presents a higher efficiency than CHC. **d** Effi-

ciency of separation and serial processing on samples to further increase total cell capture. **e** Comparison of purity between two designs. Both chips represent approximately the same purity, similar to the reports in the literature

cycles of process, while the new chip efficiency has about 45% efficiency for only one cycle, and it reaches 80% after 3 cycles. Therefore, the EHC would save processing time besides the high efficiency.

To evaluate the purity of the EHC, a test was conducted using the Re_{max} of each chip (i.e., $Re_{max}=200$ for CHC and $Re_{max}=150$ for EHC). 6 mL homogeneous mixture of 8, 15, and 20 μm particles with concentration of 100 particles per mL were used. We observed a reduction in the large particles outflow due to collisions while the high number of large particles removes smaller particles from the reservoir. Purity was calculated by dividing the number of separated 20 μm by the whole number of separated particles. As expected, the ratio of 20 μm to the total count of trapped particles in the EHC is approximately equal to the CHC. The purity of the EHC and CHC are around 80% and 78%, respectively (Fig. 6e).

5 Conclusion

Vortex technology has been widely used in size-based sorting of rare cells, being able to process the sample in a short time and with good trapping efficiency, high concentration of the sample, and high purity at very low volume. Nonetheless, the interparticle interactions and high fluid velocity are undoubtedly obstacles that do not allow all cells to enter and stay in the vortex currents. Also, increasing serialized reservoirs cause higher injection pressure that is not suitable for separating deformable cells. In this work, we examined the impact of different reservoirs height layouts on the efficiency of vortex-based systems, preferring geometries that encourage the splitting of the trapped particles and reduce the rate of vortex flow and

increase the particle trapping with decreasing serialized reservoirs and injection pressure. In addition, the asymmetric structure of the channel causes the formation of a different stable of rotation orbits and lowers the possibility of impact between particles and their release, which was proved in our simulation results and experimental tests. Furthermore, parameters such as shear gradient lift force, separatrix boundary width, and residence time have been investigated in this work. The Re_{max} for the conventional device was about 200, while the new device presented in this work is 150. Lowering the optimal rate will reduce the speed of particles in the reservoir area and reduce their collisions. Furthermore, the simulation shows an increase in shear gradient force as the primary function of capturing particles. Therefore, the saturation number of particles for each reservoir in the new chip increases. Also, the constant separation efficiency of 45% for cells and particles was achieved. Finally, the efficiency increased to 80% after 3 cycles of separation.

Supplementary Information The online version contains supplementary material available at <https://doi.org/10.1007/s10404-022-02553-z>.

Declarations

Conflict of interest The authors declare that they have no conflict of interest.

References

- Andreopoulou E, Yang LY, Rangel KM, Reuben JM, Hsu L, Krishnamurthy S, Valero V, Fritsche HA, Cristofanilli M (2012) Comparison of assay methods for detection of circulating tumor cells in metastatic breast cancer: AdnaGen AdnaTest BreastCancer Select/Detect™ versus Veridex Cell Search™ system. *Int J Cancer*. <https://doi.org/10.1002/ijc.26111>
- Bankó P, Lee SY, Nagygyörgy V, Zrínyi M, Chae CH, Cho DH, Telkes A (2019) Technologies for circulating tumor cell separation from whole blood. *J Hematol Oncol*. <https://doi.org/10.1186/s13045-019-0735-4>
- Castro-Giner F, Aceto N (2020) Tracking cancer progression: from circulating tumor cells to metastasis. *Genome Med*. <https://doi.org/10.1186/s13073-020-00728-3>
- Che J, Mach AJ, Go DE, Talati I, Ying Y, Rao J, Kulkarni RP, Di Carlo D (2013) Microfluidic purification and concentration of malignant pleural effusions for improved molecular and cytomorphological diagnostics. *PLoS One*. <https://doi.org/10.1371/journal.pone.0078194>
- Che J, Yu V, Dhar M, Renier C, Matsumoto M, Heirich K, Garon EB, Goldman J, Rao J, Sledge GW (2016) Classification of large circulating tumor cells isolated with ultra-high throughput microfluidic Vortex technology. *Oncotarget*. <https://doi.org/10.18632/oncotarget.7220>
- Cheng S-B, Chen M-M, Wang Y-K, Sun Z-H, Xie M, Huang W-H (2019) Current techniques and future advance of microfluidic devices for circulating tumor cells. *TrAC Trends Anal Chem*. <https://doi.org/10.1016/j.trac.2019.06.018>
- Cho H, Kim J, Song H, Sohn KY, Jeon M, Han K-H (2018) Microfluidic technologies for circulating tumor cell isolation. *Analyst*. <https://doi.org/10.1039/C7AN01979C>
- Desitter I, Guerrouahen BS, Benali-Furet N, Wechsler J, Jänne PA, Kuang Y, Yanagita M, Wang L, Berkowitz JA, Distel RJ, Cayre YE (2011) A new device for rapid isolation by size and characterization of rare circulating tumor cells. *Anticancer Res* 31(2):427–441
- Dhar M, Wong J, Karimi A, Che J, Renier C, Matsumoto M, Triboulet M, Garon EB, Goldman JW, Rettig MB (2015) High efficiency vortex trapping of circulating tumor cells. *Biomicrofluidics*. <https://doi.org/10.1063/1.4937895>
- Di Carlo D (2009) Inertial microfluidics. *Lab Chip*. <https://doi.org/10.1039/B912547G>
- Liu N, Petchakup C, Tay HM, Li KHH, Hou HW (2019a) Spiral inertial microfluidics for cell separation and biomedical applications. In: Tokeshi M (ed) *Applications of microfluidic systems in biology and medicine*. Bioanalysis, vol 7. Springer, Singapore. https://doi.org/10.1007/978-981-13-6229-3_5
- Haddadi H, Di Carlo D (2017) Inertial flow of a dilute suspension over cavities in a microchannel. *J Fluid Mech*. <https://doi.org/10.1017/jfm.2016.709>
- Haddadi H, Naghsh-Nilchi H, Di Carlo D (2018) Separation of cancer cells using vortical microfluidic flows. *Biomicrofluidics*. <https://doi.org/10.1063/1.5009037>
- Hur SC, Mach AJ, Di Carlo D (2011) High-throughput size-based rare cell enrichment using microscale vortices. *Biomicrofluidics*. <https://doi.org/10.1063/1.3576780>
- Jiang M, Qian S, Liu Z (2018) Fully resolved simulation of single-particle dynamics in a microcavity. *Microfluid Nanofluid*. <https://doi.org/10.1007/s10404-018-2166-x>
- Karabacak NM, Spuhler PS, Fachin F, Lim EJ, Pai V, Ozkumur E, Martel JM, Kojic N, Smith K, Chen P-I (2014) Microfluidic, marker-free isolation of circulating tumor cells from blood samples. *Nat Protoc*. <https://doi.org/10.1038/nprot.2014.044>
- Khojah R, Stoutamore R, Di Carlo D (2017) Size-tunable microvortex capture of rare cells. *Lab Chip*. <https://doi.org/10.1039/C7LC00355B>
- Lemaire CA, Liu SZ, Wilkerson CL, Ramani VC, Barzani NA, Huang K-W, Che J, Chiu MW, Vuppapalaty M, Dimmick AM (2018) Fast and label-free isolation of circulating tumor cells from blood: from a research microfluidic platform to an automated fluidic instrument, VTX-1 liquid biopsy system. *SLAS Technol Transl Life Sci Innov*. <https://doi.org/10.1177/2F2472630317738698>
- Liu C, Xue C, Sun J, Hu G (2016) A generalized formula for inertial lift on a sphere in microchannels. *Lab Chip*. <https://doi.org/10.1039/C5SLC01522G>
- Mach AJ, Kim JH, Arshi A, Hur SC, Di Carlo D (2011) Automated cellular sample preparation using a Centrifuge-on-a-Chip. *Lab Chip*. <https://doi.org/10.1039/C1LC20330D>
- Païè P, Che J, Di Carlo D (2017) Effect of reservoir geometry on vortex trapping of cancer cells. *Microfluid Nanofluid*. <https://doi.org/10.1007/s10404-017-1942-3>
- Racila E, Euhus D, Weiss AJ, Rao C, McConnell J, Terstappen LW, Uhr JW (1998) Detection and characterization of carcinoma cells in the blood. *Proc Natl Acad Sci*. <https://doi.org/10.1073/pnas.95.8.4589>
- Rastogi N, Seth P, Bhat R, Sen P (2021) Vortex chip incorporating an orthogonal turn for size-based isolation of circulating cells. *Anal Chim Acta*. <https://doi.org/10.1016/j.aca.2021.338423>
- Riethdorf S, Fritsche H, Müller V, Rau T, Schindlbeck C, Rack B, Janni W, Coith C, Beck K, Jänicke F (2007) Detection of circulating tumor cells in peripheral blood of patients with metastatic breast cancer: a validation study of the Cell Search system. *Clin Cancer Res*. <https://doi.org/10.1158/1078-0432.CCR-06-1695>

- Rostami P, Kashaninejad N, Moshksayan K, Saidi MS, Firoozabadi B, Nguyen N-T (2019b) Novel approaches in cancer management with circulating tumor cell clusters. *J Sci Adv Mater Devices*. <https://doi.org/10.1016/j.jsamd.2019.01.006>
- Shen Z, Wu A, Chen X (2017) Current detection technologies for circulating tumor cells. *Chem Soc Rev*. <https://doi.org/10.1039/C6CS00803H>
- Shen F, Xu M, Zhou B, Wang Z, Liu Z (2018a) Effects of geometry factors on microvortices evolution in confined square microcavities. *Microfluid Nanofluid*. <https://doi.org/10.1007/s10404-018-2056-2>
- Shen F, Xue S, Zhou B, Xu M, Xiao P, Liu Z (2018b) Evolution of single-particle recirculating orbits within a hydrodynamic microvortex. *J Micromech Microeng*. <https://doi.org/10.1088/1361-6439/aac02d>
- Sollier E, Go DE, Che J, Gossett DR, O'Byrne S, Weaver WM, Kummer N, Rettig M, Goldman J, Nickols N (2014) Size-selective collection of circulating tumor cells using Vortex technology. *Lab Chip*. <https://doi.org/10.1039/C3LC50689D>
- Volpe A, Paiè P, Ancona A, Osellame R (2019) Polymeric fully inertial lab-on-a-chip with enhanced-throughput sorting capabilities. *Microfluid Nanofluid*. <https://doi.org/10.1007/s10404-019-2206-1>
- Vona G, Sabile A, Louha M, Sitruk V, Romana S, Schütze K, Capron F, Franco D, Pazzagli M, Vekemans MJTA (2000) Isolation by size of epithelial tumor cells: a new method for the immunomorphological and molecular characterization of circulating tumor cells. *Am J Pathol*. [https://doi.org/10.1016/S0002-9440\(10\)64706-2](https://doi.org/10.1016/S0002-9440(10)64706-2)
- Wang X, Zhou J, Papautsky I (2013) Vortex-aided inertial microfluidic device for continuous particle separation with high size-selectivity, efficiency, and purity. *Biomicrofluidics*. <https://doi.org/10.1142/S2339547816400112>
- Wang X, Yang X, Papautsky I (2016) An integrated inertial microfluidic vortex sorter for tunable sorting and purification of cells. *Technology*. <https://doi.org/10.1142/S2339547816400112>
- Warkiani ME, Guan G, Luan KB, Lee WC, Bhagat AAS, Chaudhuri PK, Tan DS-W, Lim WT, Lee SC, Chen PC (2014) Slanted spiral microfluidics for the ultra-fast, label-free isolation of circulating tumor cells. *Lab Chip*. <https://doi.org/10.1039/C3LC50617G>
- Zhou J, Kasper S, Papautsky I (2013) Enhanced size-dependent trapping of particles using microvortices. *Microfluid Nanofluid*. <https://doi.org/10.1007/2Fs10404-013-1176-y>

Publisher's Note Springer Nature remains neutral with regard to jurisdictional claims in published maps and institutional affiliations.